

Hot spots and labyrinths: Why neuromodulation devices for episodic migraine should be personalized

Markus A Dahlem^{1,2,†}, Bernd Schmidt¹, Ingo Bojak³, Sebastian Boie⁴, Frederike Kneer⁵, Nouchine Hadjikhani^{6,7}, and Jürgen Kurths^{8,9}

¹Department of Physics, Humboldt-Universität zu Berlin, Berlin, Germany.

²Department of Biological Physik, Max Planck Institute for the Physics of Complex Systems, Dresden, Germany.

³Cybernetics Research Group, School of Systems Engineering, University of Reading, Reading, UK.

⁴Department of Mathematics, The University of Auckland, Auckland, New Zealand.

⁵Department of Software Engineering and Theoretical Computer Science, Technische Universität Berlin, Berlin, Germany.

⁶Martinos Center for Biomedical Imaging, Massachusetts General Hospital, Harvard Medical School, Charlestown, Massachusetts, USA.

⁷GNC, Sahlgrenska Academy, University of Gothenburg, Sweden.

⁸Potsdam Institute for Climate Impact Research, 14473 Potsdam, Germany.

⁹Institute for Complex Systems and Mathematical Biology, University of Aberdeen, Aberdeen AB24 3UE, United Kingdom.

†Corresponding author; dahlem@pks.mpg.de

ABSTRACT

Stimulation protocols for medical devices should be rationally designed. For episodic migraine with aura we outline model-based design strategies towards preventive and acute therapies using stereotactic neuromodulation. To this end, we regard a localized spreading depression (SD) wave segment as a central element in migraine pathophysiology. To describe nucleation and propagation features of the SD wave segment, we define the new concepts of cortical hot spots and labyrinths, respectively. In particular, we firstly focus exclusively on curvature-induced dynamical properties by studying a generic reaction-diffusion model of SD on the folded cortical surface. This surface is described with increasing level of details, including finally personalized simulations using patient's magnetic resonance imaging (MRI) scanner readings. At this stage, the only relevant factor that can modulate nucleation and propagation paths is the Gaussian curvature, which has the advantage of being rather readily accessible by MRI. We conclude with discussing further anatomical factors, such as areal, laminar, and cellular heterogeneity, that in addition to and in relation to Gaussian curvature determine the generalized concept of cortical hot spots and labyrinths as target structures for neuromodulation. Our numerical simulations suggest that these target structures are like fingerprints, they are individual features of each migraine sufferer. The goal in the future will be to provide individualized neural tissue simulations. These simulations should predict the clinical data and therefore can also serve as a test bed for exploring stereotactic neuromodulation.

Keywords: migraine, reaction-diffusion, spreading depression, gyrification, neuromodulation

1 INTRODUCTION

Migraine is characterized by recurrent episodes of head pain, often unilateral, with a prevalence of about 14% in the population, and up to 18% in women (Stovner et al., 2007). In one third of the cases migraine involves additional neurological symptoms, called aura. The neuronal

correlate of the aura is spreading depression (SD), a propagating wave of massive disruption in cortical ion and water homeostasis. In the aftermath, SD may also cause the migraine pain by an inflammatory signaling cascade from metabolically stressed neurons to trigeminal afferents in the dura (Karatas et al., 2013).

Based upon migraine aura symptoms reports like those shown in Fig. 1, it has been questioned whether SD spreads concentrically in all directions (Wilkinson, 2004). Instead it was suggested that SD in the human cortex propagates as a localized small wave segment following only one direction (Dahlem and Müller, 2004; Dahlem and Chronicle, 2004; Dahlem and Hadjikhani, 2009). A spatially more restricted SD pattern could result in less symptomatic expression and resolve why such a profound electrophysiological event, which SD clearly is, causes rather minor neurological symptoms (Charles and Baca, 2013). If that is the case, there should be an entirely new approach selectively targeting the specific paths of the SD wave segment and thus limiting its noxious effects.

There is strong evidence for localized SD patterns from five different lines of investigation. First, the spatio-temporal development of migraine aura symptoms in the visual field is often localized (Pöppel, 1973; Grüsser, 1995; Wilkinson, 2004; Dahlem and Hadjikhani, 2009; Hansen et al., 2013). This regards retinotopy as a single sensory modality (Fig. 1a,b). Second, aura symptoms follow distinct though from attack to attack variable paths when mapped onto the cortical surface across sensory and cognitive modalities (Vincent and Hadjikhani, 2007). Third, we previously suggested a mechanism in a generic mathematical reaction-diffusion model (Dahlem and Isele, 2013; Dahlem, 2013) that can explain the large variety of SD patterns observed (Hansen et al., 2013) as large-amplitude fluctuations that are critically slowed down. This mechanism links the fact that SD patterns in migraine are transient to spatial confinement in the shape of wave segments. This mechanism also proposes the existence of a more global inhibitory signal—likely established by neurovascular coupling—that merely modulates the spread of SD though it can easily be confused for SD in noninvasive imaging depending on blood flow. Fourth, we investigated how localized patterns are influenced and possibly stabilized by the intrinsic curvature of the medium using a torus (Kneer et al., 2014). To a certain degree cut outs of toroidal surfaces can approximate the hills and valleys of cortical gyri and sulci. And finally fifth, we detected localized and also re-entry and other propagation patterns of SD in

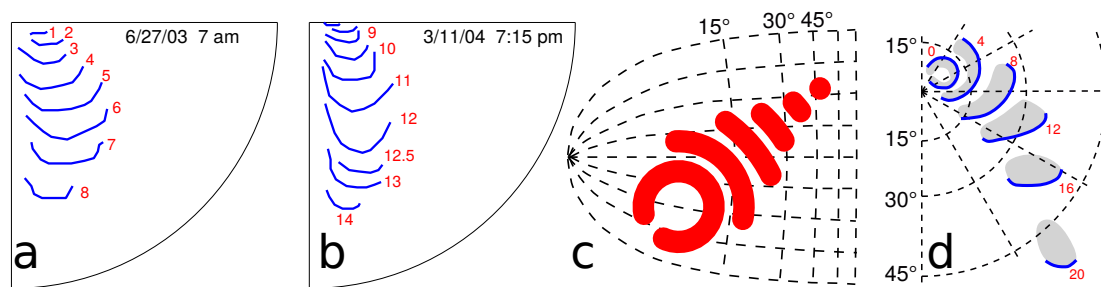


Figure 1. Empirical and postulated propagating visual field defects. (a), (b) Two similar propagation patterns of self-reported visual field defects during migraine with aura; the attacks were 258 days apart. The red number indicate time in minutes starting from the first recognition of the migraine aura phase. (c) Kinematical description of SD wave pattern in the left primary visual cortex (V1). The V1 surface is assumed flat and described by the layout of visual field coordinates. (d) Right visual hemifield with the progressive wave pattern that matches the SD pattern in (c). Red number give time in minutes. (c),(d) are modified from Dahlem and Müller (2003).

the gyrencephalic brain using intrinsic optical imaging in animal models (Dahlem et al., 2010; Santos et al., 2014).

These independent lines of evidence are integrated in this study, and further numerical simulations are performed to engage in a new model-based therapeutic brain stimulation approach. The ultimate goal of this approach is (i) to prevent nucleation of SD by spatially targeted lowering of cortical susceptibility, (ii) to shorten the transient decay time of SD, and (iii) to speed up the recovery from the aftermath of SD or even completely suppress long-lasting pain states (i.e., trigeminal or central sensitization). To conceptualize these therapeutic goals, we first describe cortical ‘hot spots’ and ‘labyrinths’ as mainly geometrical configurations that together with the areal, laminar, and cellular heterogeneity of the cortex influence the localized SD pattern formation in the human gyrified cortex in a systematic way. We suggest to consider hot spots and labyrinth paths as target structures in future stereotactic neuromodulation approaches. Our first simulations provide the direction toward large-scale neural tissue simulations as a test bed for exploring the development and quality assurance of such approaches.

2 METHODS

2.1 Mathematical model of wave segments

There is a large set of literature on reaction-diffusion (RD) models in SD (Tuckwell and Miura, 1978; Tuckwell, 1981; Almeida et al., 2004; Miura et al., 2007; Postnov et al., 2009, 2012). In this study, we used a generic model with generic rate functions. The model and its physiological interpretation can be found in a detailed review by Zandt et al. (2015) [available on request]. Briefly, the model is of activator-inhibitor type. The activator u describes the front propagation of SD, u can diffuse in the medium, and the diffusion coefficient is D . The inhibitor v is responsible for the recovery phase (spatial confinement in 1D) and for the shape in form of wave segments (spatial confinement in 2D). The latter is achieved by inhibitory global feedback described by the integral term, cf. Krischer and Mikhailov (1994). This term is proportional to surface area of the cortex being invaded by SD multiplied by the coupling strength k . The function $H(\cdot)$ is the Heaviside step function. This yields

$$\frac{\partial u}{\partial t} = u - \frac{1}{3}u^3 - v + D\nabla^2 u, \quad (1)$$

$$\frac{\partial v}{\partial t} = \varepsilon \left(u + \beta + k \int H(u) d\alpha_1 d\alpha_2 \right). \quad (2)$$

Further parameters are ε and β , the time scale separation between activator u and inhibitor v , and a threshold parameter, respectively. The independent variables α_1 and α_2 are the two spatial coordinates of the cortical surface.

Two remarks about this model are due. First, without inhibitory global feedback ($k = 0$), the RD model still can describe SD propagation as an engulfing ring-shaped wave, or, in the case of an open wave front, as a re-entry wave in the shape of a spiral (Dahlem et al., 2010). Stable localized wave segments do not exist for $k = 0$. Second, for ($k \neq 0$) stable wave solutions exist in the shape of a wave segment and these solutions are stationary solution in a comoving frame (in other words, the shape is time-independent, they are usually not ‘breathing’ structures.). Therefore it can be concluded that wave segments are also solutions of the system with $k = 0$ for a particular value of β , because the integral term is constant and only adds to the numerical value of β in this case. We rely on this in some of the arguments below. The details have been explained more rigorously and we have to refer the interested reader to these previous studies (Dahlem et al., 2010; Dahlem and Isele, 2013; Dahlem, 2013; Kneer et al., 2014). There, it has been shown that the stable wave segments in systems with $k \neq 0$ correspond in another system

with different β and $k = 0$ to unstable nucleation solutions. Moreover, there are also unstable nucleation solutions for $k \neq 0$ that evolve into a wave segment when perturbed accordingly. This behavior has also been described in detail in the literature for the model given by Eq. (1)-(2) and by similar RD systems (Krischer and Mikhailov, 1994; Bode and Purwins, 1995; Schenk et al., 1997).

In order to study the influence of the curvature on the stability of waves segments, the Laplace operator ∇^2 must be replaced with the Laplace-Beltrami operator Δ_{LB} (Davydov et al., 2003) for surfaces given in a coordinate system (α_1, α_2) :

$$\Delta_{LB} = \sum_{i,j=1}^2 g^{-\frac{1}{2}} \frac{\partial}{\partial \alpha^i} \left(g^{\frac{1}{2}} g^{ij} \frac{\partial}{\partial \alpha^j} \right) \quad (3)$$

The nucleation on curved surfaces of this RD model has been introduced by Kneer et al. (2014). Various other RD systems have also been studied in experiments and theory (Maselko and Showalter, 1989; Abramychev et al., 1990; Davydov and Zykov, 1991, 1993; Mikhailov et al., 1994; Davydov et al., 2000b,a, 2002; Manz et al., 2003; Manz and Müller, 2003).

The wave segment pattern in Fig. 1c is given by an analytic expression that was derived for kinematic approximation of the RD system for $k = 0$, and its retinotopic representation is shown in Fig. 1d, as described by Dahlem and Müller (2003).

2.2 Simplified surface construction and simulation

The surface construction of the gross morphology of the calcarine sulcus (CS) has been described by Dahlem and Tusch (2012). The smaller gyral folds and sulci indents that give rise to a random ondulation of this surface have been generated using the software package OpenFOAM (OpenCFD Ltd (ESI Group), 2014). The domain is created by the build-in tool blockMesh. The simulations were performed on a domain which has a local bump centered at the origin and a surrounding region which is flat. The bottom of the domain is given by the rotational symmetric function

$$h_b(r) = \begin{cases} 20 \cos^2 \left(\frac{\pi r}{40} \right) & r \in [0, 20], \\ 0 & \text{else.} \end{cases} \quad (4)$$

The top is generated by the constraint of a thickness of one spatial unit. The entire domain has a thickness of one layer and no flux boundary conditions at the top and bottom of the domain. This system can easily be extended to model varying thicknesses, cf. Sect. Conclusion. The system of equations has a local reaction part and the activator diffuses along the domain. The time derivatives are being discretized by an implicit Crank-Nicholson scheme.

The spatial part is dissected into control volumes leading to a discretization of the computational domain. Inside a control volume the gradient of the flux is approximated using central differencing around the nodal point in the center of the control volume. The control volumes are coupled via the flux between the interfaces of adjacent control volumes. Periodic boundary conditions are applied at the boundary of the domain to mimic an infinitely large domain. However only single interactions with a local bump were studied. Details of the method are described in (Versteeg and Malalasekera, 1995).

To generate wave segments the following procedure has been adhered to. For $k = 0$, the model allows for a stable planar pulse propagation in one spatial dimension. An excited initial area (activator equal to one) that spans the entire height of the domain has been generated as initial condition. Such a pulse would spread to the left and right. To break the symmetry the area to the left of the activated area is inhibited (inhibitor variable equal to 0.5). After about 800 time steps a smooth stable pulse propagates to the right. Open ends are created by setting

the activator and inhibitor concentration to the equilibrium state at the top and bottom ends of the pulse solution. Only then k is set to its nonzero value and the wave segment is stabilized. After about 1000 time steps all transients dynamics or damped out and the stable wave segment propagates to the right. The parameter values used to model the system described by Eq. (1)-(2) are $\varepsilon = 0.04$, $D = 1$, $\beta = 0.9$ and $k = 0.003$. In the last step, the stable wave segment is mapped onto a domain with a bump with varying parameter d . The value of the angle ϕ is measured after the wave segment as passed the pump completely.

2.3 Matching simulations of migraine aura on individual MRI scans

Anatomically and geometrically accurate representations of the cortex are needed for realistic modelling of SD nucleation and propagation. Furthermore, spatially targeted clinical applications require the extraction of the cortical surface in every individual case, given the considerable variation of the folds and the boundaries of brain areas in the human brain. Structural MRI data can be used to distinguish different tissue types with sufficient spatial resolution, and various open-source and commercial software tools exist for automatic MRI tissue segmentation and mesh generation, including FreeSurfer (Dale et al., 1999; Fischl et al., 1999) and FSL (Smith et al., 2004).

A left V1 surface was obtained by magnetic resonance imaging (MRI) from a migraine sufferer who fulfills the International Headache Society criteria for the diagnosis of migraine with aura, for details see the study by Dahlem and Hadjikhani (2009). We customize and validate the traveling wave patterns of migraine aura pathophysiology by uploading the MRI scanner readings into our self-programmed simulation tool box that uses a C++ software library supporting the creation of finite element codes (Bangerth et al., 2007). The methods involve an automated conversion of 2D triangular mesh from the fMRI into a quadrilateral mesh, for later adaptive refinement and coarsening by the software library.

To generate stable wave segments as an initial condition, we proceeded in a very similar way as described for the scattering simulations at smaller gyral folds and sulci indents above. The parameter values used to model the system described by Eq. (1)-(2) are $\varepsilon = 0.04$, $D = 1$, $\beta = 1.2$ and $k = 0.0045$. Note the change in β and k compared to the simulation on the surface with a bump. These different values select a solution of a wave segment with different size to better match the aura symptoms. The main difference in this case is that we have to project this stable solution from a flat surface onto the intrinsically curved V1 surface. There is not a straightforward way to calculate a natural initial condition, because there is no stationary shape on a surface with varying curvature. Even on a flat cortex the natural initial conditions (conditions that ignite SD in the cortex) probably correspond to random spatial patterns caused by some large fluctuation in either metabolic energy supply or neural activity or in both. We addressed this problem using cortical feature maps in V1 (Dahlem and Isele, 2013). For our simulations here, the initial conditions had to satisfy the correct initial propagation direction to match the visual field defects shown in Fig. 1a,b, which was drawn from the visual field defects as described by Hansen et al. (2013).

2.4 Gaussian curvature K for a discretised cortical surface

To determine the Gaussian curvature, we use a cortical surface originally extracted with CIVET (Kim et al., 2005). This surface consists of 163,840 triangles with 81,924 vertices in two separate closed hemispheres, where each of the mesh vertices can be considered as representing the surrounding neural tissue and its connectivity (Bojak et al., 2010, 2011).

A variety of methods have been proposed for the estimation of curvature from such discretised mesh surfaces, see the review of Magid et al. (2007). An extensive investigation of these methods is beyond the scope of this article. Magid et al. (2007) identify fitting osculating paraboloids

as the method of choice if one wants to employ only one method, due to its good stability, convergence and accuracy. This method also has the advantage of conceptual simplicity and computational speed. Essentially, to compute the curvatures at a specific vertex, its coordinates and those of its immediate neighbours are transformed by translation and rotation so that the vertex is now located at the origin and the surface normal at the target vertex coalesces with the z -axis. This surface normal can be estimated as the average of the normals of the triangles that the vertex forms with its neighbours. Then a least square fit of the canonical parabolic form $z = ax^2 + bxy + cy^2$ to the vertex and its surrounding neighbours is performed, making the resulting paraboloid optimally osculate, i.e., be as near as possible to all these vertices. From the resulting fit values the mean $H = a + c$ and Gaussian $K = 4ac - b^2$ curvatures, respectively, can be obtained directly. If needed, the principal curvatures $\kappa_{1,2} = H \pm \sqrt{H^2 - K}$ are easily computed from these values. Overall, the method hence consists in estimating the curvatures at a mesh point by identifying them with the curvatures of a locally fitted paraboloid.

In practice, mesh surfaces obtained from MRI tissue segmentation are uneven at the scales of the original voxels, since the tissue interfaces may pass through a voxel at various levels and angles, and in addition can suffer from overfitting leading to artificial ripples in the extracted surfaces. To guard against overestimating the curvature due to such artefacts, we have employed the following procedure here: We estimate the curvature not only from the vertex and its surrounding ring of nearest neighbours (yielding H and K), but also from the same vertex and the surrounding ring of next-to-nearest neighbours (yielding \tilde{H} and \tilde{K}), i.e, from target vertex and the ring formed by the neighbours of the neighbours of the target vertex, where that ring obviously excludes the target vertex itself. We now consider the difference of these estimates $\delta H = H - \tilde{H}$ and $\delta K = K - \tilde{K}$, respectively, across all $n = 81,924$ vertices and use Chauvenet's criterion to detect outliers in these differences: Given the mean $\mu_{\delta H}$ and standard deviation $\sigma_{\delta H}$ of the δH , we consider as outliers those points where $n \cdot \text{erfc}(|\delta H - \mu_{\delta H}|/\sigma_{\delta H}) < 0.5$. At regular points we use the H , whereas at outlier points we use whichever value is smaller, H or \tilde{H} . The same procedure is used to determine whether K or \tilde{K} should be used. This method provides a conservative estimate of the curvature suppressing local artefacts. For the particular surface used here, 1.4% of vertices were outliers in H , and 0.8% in K , thus the surface for the most part proved to be smooth.

In Fig. 5 we show the result for our cortical surface. The actual range of values is $-2.343/\text{mm} \leq K \leq 2.429/\text{mm}$. However, to enhance the visibility of the mostly small curvature of cortex, we show $\kappa_{\text{geo}} \equiv \text{sign}(K)\sqrt{|K|}$ on a color scale $[-1.56/\text{mm}, 1.56/\text{mm}]$, as indicated by the color bar. κ_{geo} is basically the *geometric* mean of the principal curvatures κ_1 and κ_2 , and the Gaussian curvature $K = \text{sign}(\kappa_{\text{geo}})\kappa_{\text{geo}}^2$. From right to left in Fig. 5, we zoom in on the spot with largest negative Gaussian curvature $K = -2.343/\text{mm}$ in two steps, as indicated by the orange and yellow boxes, respectively. One can clearly see that this potential nucleation point is buried deep in a sulcus of the visual cortex. We discuss these results further below.

3 RESULTS

3.1 Cortical hot spots and principal effects of Gaussian curvature

The principal idea of cortical 'hot spots' and paths that span cortical 'labyrinths' is firstly illustrated in a simplified way. We describe them as anatomical landmarks with a particular geometrical configuration. We separately take into account the gross morphology of the calcarine sulcus (CS) and smaller gyral folds and sulci indents that give rise to a random undulation of the CS surface.

3.1.1 Gross morphology of the calcarine sulcus

The CS is a reliable landmark of the primary visual cortex (V1). Visual migraine auras often originate in V1 or in higher visual areas neighboring V1 (Fig. 1). Therefore CS can be considered a typical fold in which many migraine auras originate and travel through.

CS is a cortical fold formed by the cuneus and lingual gyrus on the medial surface and runs forward to the corpus callosum (Fig. 1a). The fundus of CS is, roughly speaking, the curve of maximum depth that then further spans the length of CS. The surface area of V1, which lies in CS, can, for example, easily be identified post-mortem by the stria of Gennari, i.e., a band of myelinated axons (see Fig. 2b,c).

The dorsal and ventral banks of CS can be heavily ramified with smaller gyral folds and sulci indents. To illustrate the main folding pattern with respect to the visual field coordinates (Fig. 2e,f), the CS surface has been streamlined (Dahlem and Tusch, 2012). A real example is considered in detail in Sec. 3.2. On the streamlined model surface (light blue in Fig. 2e) the entrance of CS is a saddle surface. It has negative Gaussian curvature (blue, see Fig. 2g). Farther down CS, when the fundus almost reaches its maximum depth, the Gaussian curvature becomes positive (red). Elsewhere, the Gaussian curvature is very close to zero or zero (gray).

We suggest to consider regions with large absolute values of negative Gaussian curvature, such as at point A in Fig. 2g, as cortical hot spots of SD generation. This follows from previous studies that showed that negative Gaussian curvature causes a smaller nucleation barrier for reaction diffusion waves such as SD (Kneer et al., 2014). Therefore, these areas can more easily lead to subsequent autocatalytic growth of seeds caused by the spatio-temporal fluctuation in homeostatic control.

We also showed that unstable nucleation solutions in a flat medium can be stabilized by the negative gradient of Gaussian curvature on the outside of a torus (Kneer et al., 2014). This provides an alternative mechanism of wave segment creation. A surface similar to the outside of a torus is assumed when the fundus almost reaches the maximum depth of CS at point B in Fig. 2g. Note that gyral crowns are also of similar shape and the Gaussian curvature does not distinguish between gyrus and sulcus (cf. Sect. Conclusion).

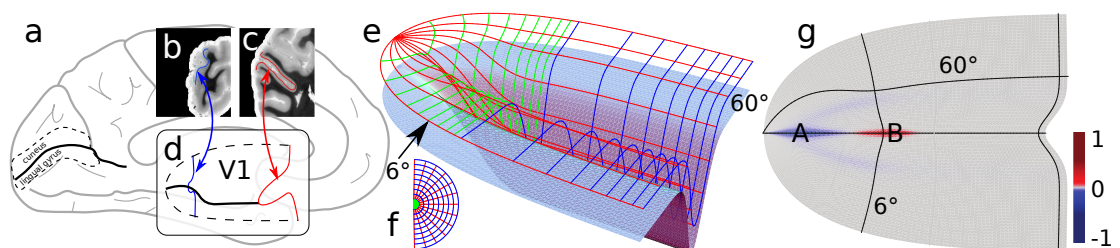


Figure 2. Principal folding pattern correlating with a cortical area defined by a functional field. Modified from study by Dahlem and Tusch (2012). (a) Medial side of the brain. One the occipital pole to the left, the calcarine sulcus is marked (think black line). (b)-(c) Coronal section through the occipital pole. Blue and red line traces the stria of Gennari as a marker of the primary visual cortex (V1), which is outlined in (a) by a dashed line. (d) Gross 3D shape of V1, about two-thirds of the surface area lie within the CS walls. The ventral and dorsal half of V1 are assumed to be symmetric with respect to the fundus, in particular, they extend equally long into the anterior direction, the shape of the walls are approximated with smooth profiles (see study by Dahlem and Tusch (2012) for details). (e) Light blue surface as in (d) with the retinotopic grid on top. (f) Visual field polar coordinates. (g) Gaussian curvature of V1.

3.1.2 Single sulci indent

Before we consider in detail the influence of randomly changing negative and positive Gaussian curvature in real cortical surfaces, we describe the influence of a single sulci indent on an otherwise flat surface. Indents rather small in extent (diameter) but relatively large altitude are not unusual, in particular in the deep sulci of the occipital pole. The flat surface can be thought of as either the dorsal or ventral bank of CS.

In Fig. 3, we show the scattering effect of a local bump, representing a small sulci indent, on a travelling stable wave segment. Whether stable wave segments were deflected by positive or negative angles ϕ (Fig. 3a) depends in a systematic way on the offset d (Fig. 3b). In the example shown in Fig. 3c-h the stable wave segment is deflected by a positive angle ϕ . This can intuitively be understood. The near side of the wave segment, with respect to the bump location, has to travel a longer distance and therefore falls behind. The net effect is then a turn towards the bump indicated by a positive angle ϕ . This, however, is easy explanation is only correct to a medium range of d between value 5 and 15.

For a direct collision ($d = 0$) or too small an offset ($d < 5$), however, the stable wave segment can even get eradicated (Fig. 3i-q). We call a wave-bump interaction in this range that eradicates the wave segment a head-on collision. For example, the wave disappears a few time steps after the snapshot shown in Fig. 3q. A bump always causes first a negative Gaussian curvature and then the sign of the Gaussian curvature changes (indicated by the dashed line Fig. 3a) and the bump surface assumes a positive Gaussian curvature. The critical effect that causes the wave segment to vanish is due to large size and shape variations. These in turn are due to the rapidly changing gradients in Gaussian curvature in a head-on collision. Note that the size variations continue long after the bump is passed. This oscillation is called ‘breathing’. It indicates that wave segment is a stable focus in phase space (Strogatz, 1994). The perturbation in a head-on collision, however, has kicked the system out of the basin of attraction of the stable focus. For much smaller bumps (lower altitude) interactions even for $d = 0$ will only cause perturbation inside the basin of attraction and therefore not eradicate the wave segment. These would consequently then not be called a head-on collision, because the segment survives unchanged though it performs damped breathing.

Let us briefly describe the mechanism that actually destroys the wave outside the basin of attraction. For too large an amplitude of the subsequent breathing, propagation is not possible anymore because the wave size gets too large. The wave size shown in Fig. 3q is a last deep

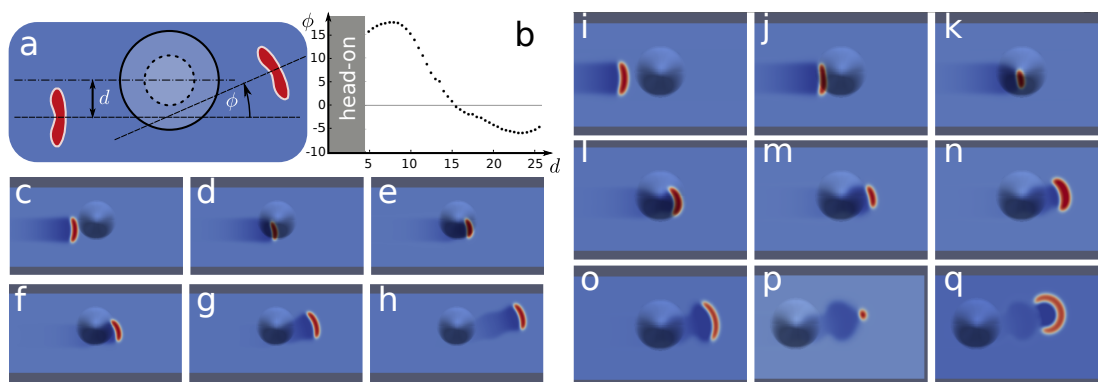


Figure 3. Wave segments deflected by a bump. (a) Scheme with definitions of offset parameter d and deflection angle ϕ . (b) Deflection angle ϕ versus offset d . (c)-(h) Numerical simulation of a positive deflection. (i)-(q) Numerical simulation of head-on collision with wave destruction.

gasp close to the final frontier called propagation boundary, see the review by Zandt et al. (2015) and references therein for details. Briefly, a large wave size leads to increased threshold β by global inhibitory feedback described in Eq. 2. Above this well-defined value of the threshold the propagation becomes impossible. The global inhibitory feedback could stem from dilations of surface vessels in regions that show no directly increased neural activity (Gao et al., 2014) and thus have higher resistance against SD invasion (cf. Sect. Conclusion).

For large offsets d , the deflection can be by negative angles ϕ (Fig. 3b). This can also intuitively be understood. Only the tip at the open end experiences the geometrical change. This change is by a negative Gaussian curvature. Due to the diminished surface area at negative Gaussian curvature, with respect to a flat surface, the tip can more quickly recruit the tissue. This is because in front of the tip the surface area is reduced and by an effective convergence in diffusion this tip grows more than the one on the opposite end. As a result, the wave is deflected by negative angles ϕ . The same effect also causes the smaller nucleation barrier at the location of hot spots.

3.2 Cortical labyrinths

To introduce the idea of cortical labyrinths, we use real cortical surfaces. First, we consider the cortical area V1 and a simulation of a stable wave segment on this surface. Next, we consider the whole cortical surface with its heterogeneous distribution of Gaussian curvature.

3.2.1 Individual path in V1

A left V1 surface was obtained by magnetic resonance imaging (MRI), see Sect. Methods. On this surface we simulated the path a stable wave segment takes (Fig. 4). We placed the wave segment near the occipital pole pointing toward the direction of the cunes (cf. Fig. 2a). The visual aura that is matched is within the lower quadrant of the right visual hemifield near the vertical meridian, see Fig. 1a,b. The lower quadrants of visual hemifield are mapped onto the ventral bank of CS and the cuneus, on which the vertical meridian is also represented. The initial position was estimated as the location of the neural representation of the fovea, which is located at the occipital pole often extending about 10mm onto the lateral convexity.

The path the simulated wave segment takes matches closely the path of the visual aura in the visual field within the first eight minutes of an attack at one day and within minutes 7-14 at another day (Fig. 1a,b). During these periods, it propagated within the lower visual quadrant in the right visual hemisphere from the center to the periphery and at about 8° eccentricity it disappeared or was clinically silent for seven minutes and reappeared (Dahlem and Hadjikhani, 2009). The anatomical and physiological features of this distinctive and further aura patterns of this migraine sufferer were also investigated by Hansen et al. (2013). Let us remark that because

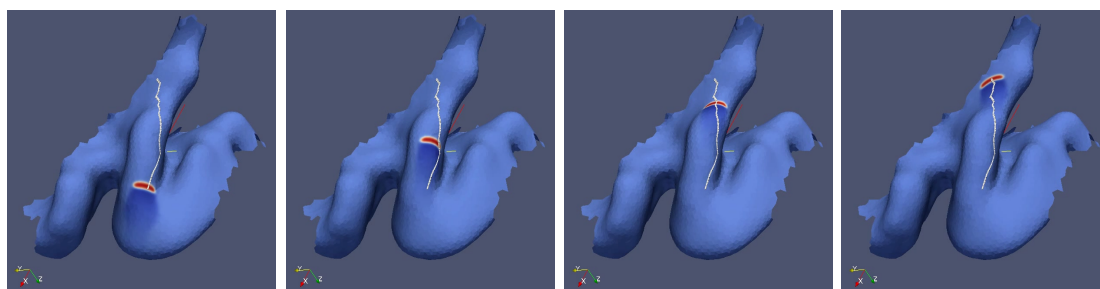


Figure 4. Simulation of spreading depression on an individually shaped cortical surface obtained by MRI from a migraine sufferer.

SD propagates with about 3mm/min, 8min correspond to a distance of about 24mm, which is about the size of the particular gyral crown on the cuneus (Fig. 4).

After we simulate the individual path in V1 of this distinctive aura attack, we can determine the start and end point. These points were given by the center of gravity of the wave segment at the respective positions. Between the start and end point, we also calculate the shortest distance path (white line in Fig. 4). It can be seen that the actual path along this wave segment travels overlaps by and large with the shortest distance path.

The idea of the shortest path can be misleading as the wave segment does not teleologically propagate to its final position. Geodesics are locally the shortest path between points in the space, but they are not necessarily the shortest path globally. The osculating plane of the geodesic line is perpendicular to the surface tangent plane, which provides a local criteria for the calculation. This criteria is probably the reason why wave segments approximately follow with their center of gravity geodesics. Yet, as shown in Sec. 3.1.2, wave segments can be deflected by small but high gyral folds and sulci indents. Such geometric objects in the path of a wave segment may not interfere with the center of gravity of the wave segment. Hence, wave segments will not exactly travel along geodesics that are defined by the center of gravity alone.

3.2.2 Distribution of Gaussian curvature and other heterogeneities

Last, we calculate the distribution of the Gaussian curvature of a whole cortical surface (Fig. 5). It can be seen that the curvature overall deviates only moderately from zero. Larger indents can be, however, in the deep sulci of the occipital pole.

It is well known that the cerebral cortex also exhibits considerable regional heterogeneity from cellular, to laminar and areal heterogeneity as briefly outlined in the discussion. Hence, it is important to estimate spatial scales of the heterogeneous distribution of Gaussian curvature in comparison. The change of sign occurs every couple of millimeters, although larger domains and connected stripes of one polarity (negative or positive value of Gaussian curvature) exist.

Ignoring for the moment any other heterogeneity, even the set of permitted geodesics starting from a given point is a complex network. Non-permitted geodesics are those that lead into dead ends due to head-on collision with unfavorable curvature conditions (in addition to other unfavorable heterogeneities, which we have for the moment ruled out, but see Sect. Conclusion). There can be several geodesics on the cortical surface between two given points, so in principle geodesics that start from the same point can later cross again (Maekawa, 1996). A geodesic is, of course, conceptually similar to a straight line in a flat geometry. Given a common start point, straight paths in a flat surface simply span radially lines. Hence curvature makes a significant

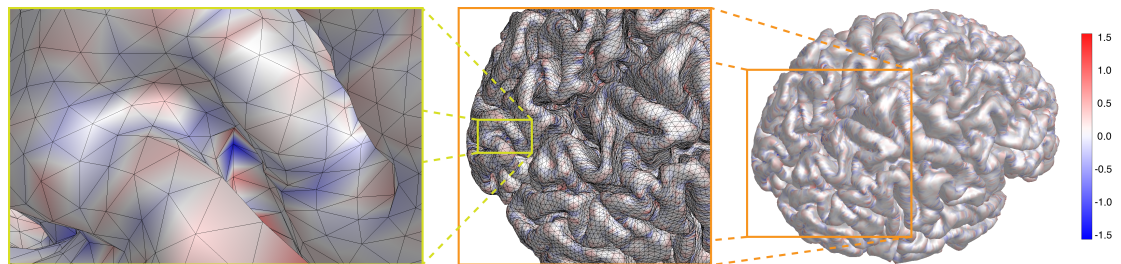


Figure 5. For a cortical surface $\kappa_{\text{geo}} \equiv \text{sign}(K) \sqrt{|K|}$ is shown on a color scale $[-1.56/\text{mm}, 1.56/\text{mm}]$, as indicated by the color bar. From right to left, the spot with largest negative Gaussian curvature $K = -2.343/\text{mm}$ is brought into focus by zooming closer twice, as indicated by the orange and yellow lines, respectively. It represents a potential nucleation point for SD.

contribution to the traveling paths that can span a labyrinth of wave segments even in the absence of other heterogeneities, which are probably at least as relevant and modify the labyrinth structure further.

To define the ‘cortical labyrinths’, we have to take into account the geodesics and further effects of the Gaussian curvature on the traveling wave segment (see Sec. 3.1.2, deflection and head-on collisions Fig. 3) as well as regional cellular, laminar, and areal heterogeneity. Without measuring or defining all the various structures and make them amenable to numerical simulations, we can always fall back to an operational definition by principle. We call a labyrinth the set of paths a wave segment with a given size can take starting from a particular location on the cortex. To calculate this is computationally expensive as labyrinths depend on the starting point and wave size (defined in flat geometry). Moreover, we currently cannot include information on regional heterogeneity in necessary detail (see Sect. Conclusion).

As this is beyond the scope of this study, let us summarize and highlight the similarity to a labyrinth structure. Wave segments can only travel on fixed paths. Some of these paths will be a dead end. The random undulation to the gross cortical morphology alone will already render the particular labyrinths an individual feature, like a fingerprint, of each migraine sufferer.

4 CONCLUSION

4.1 Regional heterogeneity in the cortex

The cerebral cortex exhibits regional heterogeneity. This not only can considerably influence the path an SD segment takes, it also actually reveals the only information we currently have about these particular paths. For both reasons, the parcelation into cortical areas as functional domains should be stressed among various other factors that introduce heterogeneity in the cortex.

4.1.1 Clinical manifestations of SD wave segments

It seems that a localized SD wave segment travels through several different cortical areas along a coordinated path in a single migraine aura attack—though from attack to attack different paths may be taken. This is inferred from the fact that migraine aura symptoms frequently occur in patterns each fitting a particular spatially aligned distribution of various successively impaired cortical functions (Vincent and Hadjikhani, 2007).

A full-scale attack is characterized according to the Headache Classification Committee of the International Headache Society by multiple sensory and/or cognitive symptoms during the aura phase. Each individual aura symptom can last up to 60 minutes, thus the acceptable maximal duration for three different symptoms is 180min or a path length of 54cm. This seems reasonable for a narrow wave segment meandering in an area of $\sim 2000\text{cm}^2$ folded and undulated cortical surface. A segment of 0.5cm width covers only $\sim 1.35\%$ of the available surface area. In contrast, an engulfing SD with a radius of 54cm would invade 3.5 times more surface area than is actually available.

4.1.2 Functional domains and anatomical landmarks

Cortical areas are defined based upon cytoarchitecture, functional studies, and subcortical connectivity. These factors can be independent. In the visual cortex, for example, except for V1, there is no correspondence between cytoarchitecture (Brodmann) and function (defined by retinotopic mapping). Of course all these heterogeneities need to be considered in addition and in relation to Gaussian curvature when trying to estimate the set of preferred paths of SD propagation. Moreover, sensory and motoric domains can have some relationship to the gross sulcal and gyral morphology. These factors are not independent. In particular, subcortical connectivity and sulcal and gyral morphology could be related by developmental mechanics (Hilgetag and Barbas, 2005). Yet, there also is substantial interindividual variability in both the

size and location (Rajkowska and Goldman-Rakic, 1995; Thompson et al., 1996; Roland and Zilles, 1998; Amunts et al., 1999).

Only in a few cases more or less precise correlations between the folding pattern and functional domains have been demonstrated. The most reliable relation is the calcarine sulcus (CS, see Fig. 2) as a landmark of the primary visual cortex (V1) (Stensaas et al., 1974; Gilissen and Zilles, 1996; Andrews et al., 1997). For visual areas outside V1, a purely anatomical identification is also quite reliable for V5, which lies at the intersection of the ascending limb of the inferior temporal sulcus and the lateral occipital sulcus (Watson et al., 1993; Walters et al., 2003). The primary auditory cortex has a clear spatial relationship with Heschl's gyrus (Gaschler-Markefski et al., 1997; Rademacher et al., 2001). All these functional domains are relevant in relation to migraine aura symptoms. Last, the motor cortex can be identified by the position of the central sulcus (Lotze et al., 2000). While this is often suggested as a barrier for an engulfing SD pattern, there is evidence that also the prefrontal cortex can be affected (Schipper et al., 2012; Borsook et al., 2014).

4.1.3 Curvature, folding, and thickness

An important fact is that with the cortical folding pattern the cytoarchitecture also varies in a systematic way. There is a crucial distinction to be made. The folding pattern is mainly determined by extrinsic curvature, while Gaussian curvature is intrinsic curvature. Simply said, the SD wave as an "inhabitant" of the cortical surface feels only intrinsic curvature directly. Extrinsic curvature can only indirectly, that is, via the cytoarchitecture, influence SD propagation. In other words, the effect by Gaussian curvature and by differences between gyral vs. sulcal convolutions are distinctively different.

Gyral convolutions of the cerebral cortex are thicker than sulcal ones, which is specifically due to an increase in the thickness of the deep layers (V+VI). The increased neuron number and increased thickness of these deep gyral layers correlate so that the density of deep layers is relatively invariant across the cortical landscape, see study by Hilgetag and Barbas (2005) and references therein. If the cell density is constant in different thicknesses of deep layers, volume fraction between intra- and extracellular space and volume-to-surface-area relation should also be invariant. These factors determine important electrophysiological properties of SD on a cellular level (Hübel et al., 2014; Hübel and Dahlem, 2014).

Notwithstanding, cortical thickness differences have been reported in migraine sufferers in two studies (Granziera et al., 2006; DaSilva et al., 2007) and the possible implications have been discussed thoroughly by Hadjikhani (2008), so that we can refer the interested reader for details to this. Briefly, focal dysplasias may render the cortex more excitable, which could then add to the effect of negative Gaussian curvature to create hot spots. The cortical thickness changes can be also a result of plasticity following repetitive episodes of pain, which may suggest that there could also be protective changes in plasticity following repetitive neuromodulation.

The central point taken away from these studies on natural and abnormal variations in cortical thickness for the current study is that the approximation of the cortical sheet as a 2D surface does not hold in all circumstances and that the problem can ultimately only be resolved in a neural tissue simulation that extends the requirements and constraints of circuit simulation methods on a cortical sheet (in the continuum limit neural fields) by creating a tissue coordinate system that allow geometrical analysis (Kozloski and Wagner, 2011).

4.1.4 Cortical grade separation

Another noteworthy heterogeneity concerns the laminar structure. Studies in rat show that cortical DC shifts associated with SD can move either in layers near the cortical surface or in deeper cortical layers below a border zone between layer IV and layer V (Richter and Lehmenkühler, 1993). Layer IV is the granular layer of the cortex which could have for SD an unfavorable

high volume-to-surface-area. There is not always a strong correlation between the time course of DC shifts in upper and lower cortical structures. It has been suggested that in human, the occurrence of SD in upper and/or deeper cortical layers could have implications on the type of the migraine attack (aura with headache, aura without headache or headache without aura) (Richter and Lehmenkühler, 1993). Grade separation would add significantly to the complexity of a labyrinth structure as at-grade intersection of a non-or-all phenomenon such as SD would cause annihilation or merging but not bypassing cross each other. Much of the anterior cortex including the prefrontal cortex, however, lacks a defined layer IV, thus the labyrinth is at-grade in an agranular cortex.

4.1.5 Vasculature

SD does not only cause a hemodynamic responses (Dreier, 2011). SD can also be caused by hemodynamic abnormalities and its propagation path can be changed by hemodynamic action. For example, large and correlated fluctuations originating from autonomic subnetworks have been suggested to occur as part of a typical tipping point behavior in the prodromal phase of migraine (Dahlem et al., 2014). These global fluctuations can ignite SD locally in a hot spot by crossing there the nucleation threshold for propagation first.

Pial vessels, which distribute blood from the cerebral arteries to the penetrating arterioles, can locally block the propagation (Santos et al., 2014). The penetrating arterioles occur about every $300\mu\text{m}$ and the pial surface artery network is an interconnected honeycomb-like mesh (Blinder et al., 2010). The regulation of cerebrovascular tone is coordinated by perivascular nerves, glia, and blood pressure and its hydraulic functions. Vessel dilations can propagate into this pial mesh also mediated by fast electrical connections between endothelial cells. In fact, surface vessels show much larger dilations than their intracortical branches and this dialation can also occur in regions that show no directly increased neural activity but are neighboring regions that do show increased activity (Gao et al., 2014). This may provide a fast and long-range inhibitory feedback, as described by Eq. 2.

It is also noteworthy that with laser speckle technology the cerebral blood flow was measured in patients with malignant hemispheric stroke after hemicraniectomy. The path of SD was visualized and this was also suggestive of a small wave segment form (Woitzik et al., 2013).

4.2 Hot spots and labyrinth paths as target structures in stereotactic neuromodulation approaches

Various treatment strategies for migraine are available today. It cannot be stressed enough that the recommended approach based upon clinical experience is an integrated headache care. Treatment of acute migraine attacks and prophylaxis is accompanied by education and counselling, behavioural therapy and treatment of co-morbidities. However, with respect to drug treatment “acute treatment and preventive therapy of migraine seems to have come to a halt recently. The last real innovation in the treatment of migraine attacks were the triptans, which were introduced 20 years ago. [...] [I]t is time to explore new avenues in the treatment of migraine” (Diener, 2013).

Computational models of migraine not only help to better understand this disease. They also help to identify new opportunities to intervene. Our results suggest that the primary objective in research relating SD to migraine pain should be directed to obtain a measure of the different noxious signatures that are transmitted into the meninges and drive the migraine-generator network into the pain state, i.e., central sensitization (Fig. 6). In this context, neuromodulation is of particular interest, because computational models can identify the accessible intervention points. For example, for the treatment of chronic migraine (>15 headache days per month) with transcranial direct current stimulation (tDCS) the current flow through subcortical brain regions

associated with pain perception and pain modulation (i.e., trigeminocervical complex (TCC), rostral ventromedial medulla (RVM), locus coeruleus (LC), and periaqueductal grey (PAG), see Fig. 6a) was estimated using a computational model (Dasilva et al., 2012).

In analogy to pharmaceutical substances, specific stimulation protocols for medical devices (Fig. 6b-d) should be approached by rational design, in particular with respect to the various pain phase of the migraine cycle (Fig. 6e). The goals are also shared with drug treatment, namely to (i) achieve fewer attacks, (ii) abort attacks at an early stage, e.g. in the prodromal or aura phase, and (iii) lessen the severity in the pain phase. To achieve these three goals our results suggests framework conditions on three strategies towards one preventive and two acute therapies with stereotactic neuromodulation for episodic migraine, such as tDCS, transcranial alternate current stimulation (tACS), and transcranial magnetic stimulation (TMS).

- (i) To achieve fewer attacks, our results suggest that one must first identify individual cortical hot spots. Targeting hot spots selectively minimizes intervention. This seems advised because the appropriate stimulation protocols have to cause lasting plastic alterations of cortical excitability. The rational is to lower susceptibility at individual hot spots to prevent nucleation of SD. This can be done with image-guided TMS sessions during the attack-free interval. The intervention probably even must be done outside ictal phase, because protocols may focally increase neural activity to induce lasting protective preconditioning-like effects that would bear negative impact in the acute phase.
- (ii) To abort attacks in the aura phase is the current rational of portable TMS devices (Fig. 6c); patients were instructed to begin treatment as soon as possible after aura symptoms where

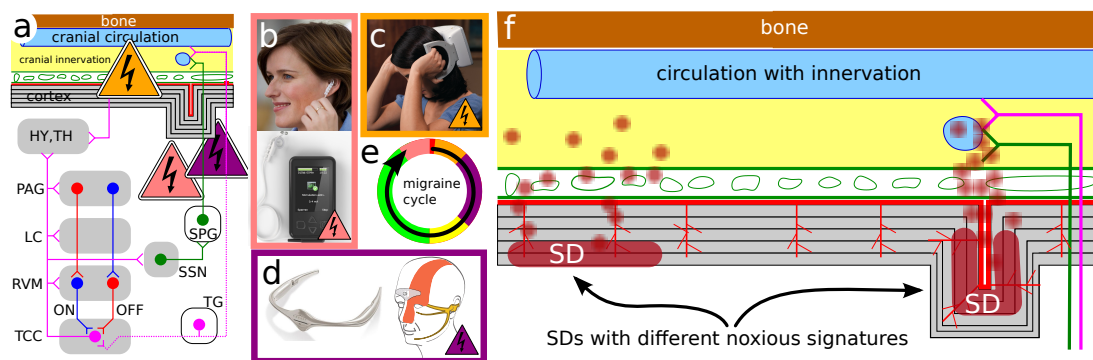


Figure 6. (a) Working model of the migraine-generator network with accessible intervention points (see text) (Dahlem, 2013). (b) Clinical studies on the effect of transcutaneous vagus nerve stimulation (tVNS) VITOS[®] and gammaCore[®] are underway and have been published (Magis et al., 2013); figure courtesy cerbotec GmbH © 2014. (c) Transcranial magnetic stimulation (TMS), SpringTMS[®] FDA-approved for episodic migraine during the aura phase; figure courtesy of eNeura Inc. © 2014. (d) External Trigeminal Nerve Stimulation (e-TNS), Cefaly[®] FDA-approved for episodic migraine prevention; courtesy of CEFALY Technology © 2014. (e) Migraine cycle: attack-free interval, average two weeks (green); prodrome, ~24h (salmon); hot spot nucleation (red) and aura phase, 60min for each symptom (orange); pain phase, 4-72h (dark violet); postdrome, ~24h (yellow). (f) Schematic representation of a cortical cross section with meninges and skull; not to scale. The effect of SD and its noxious signature could significantly vary with overall size of affected area and SD's gyral, sulcal, and laminar location. Future studies will be needed to design specific treatment stimulation protocols that take into account the noxious signature and its phase within the migraine cycle.

noticed and always within 1h of aura onset (Lipton et al., 2010). In the period after SD is ignited, previous theoretical model studies proposed that the inevitable decay of the cortical patterns is critically slowed down by a bottle-neck situation (Dahlem and Isele, 2013; Dahlem et al., 2013). Our results here suggest that these patterns are both selected and temporally stabilized by labyrinth paths. Taken together, the current two single pulse paradigm (for $\sim 0.5s$, $\sim 30s$ apart) are likely to turn with a certain success rate wave segments into faster-decay paths or dead ends. Repetitive TMS with low amplitude, however, could be more effectively shorten the transient decay time. Noise during a bottle-neck passage (Strogatz, 1994) induces large fluctuations allowing the dynamical system to explore nearby states and faster traverse the bottle-neck passages in phase space.

- (iii) To speed up the recovery from the aftermath of SD or completely suppress a long-lasting pain state (i.e., trigeminal or central sensitization) the stimulation protocol need to intervene with the inflammatory signaling cascade from metabolically stressed neurons to trigeminal afferents in the dura (Karatas et al., 2013). Our results suggest that the cascade from the brain parenchyma to the dura is effected by geometrical constraints (Fig. 6f). For example, if the labyrinth path is entirely in a sculus, sufficient concentrations of inflammatory mediators can be siphoned from the perivascular space into the subarachnoid space. One must first identify the individual cortical labyrinths to identify optimal target regions where the inflammatory cascade can be interrupted. In this context it is interesting to note that despite the gyral crown of the cortex being subjected to a larger magnetic field magnitude during TMS, the sulcal banks show larger cerebral blood flow responses (Krieg et al., 2013).

Strategies (ii) and (iii) describe early and on-demand interventions during the pre-ictal state. Aura symptoms can announce the pre-ictal state in about 30% of the cases. Yet these are not the only indicators of the pre-ictal state. Also other sensory, affective, autonomic, and cognitive functions are altered in this phase and provide means by which migraine sufferers become aware of pre-ictal ‘errors’ (Borsook et al., 2014). Strategy (i) seems more bold, as we suggest that migraine might be unlearned. Identifying cortical hot spots and cause plastic changes at these foci is but only first step towards electroceuticals (Famm et al., 2013) that are currently discussed to override pain signals or reprogram circuits from accessible intervention points (Fig. 6a).

Already, the first transcutaneous electrical nerve stimulation (TENS) device (Fig. 6d) and the first TMS device (Fig. 6c) were FDA-approved for episodic migraine for prevention and during the aura phase, respectively. Other neuromodulation including invasive methods are approved only for chronic migraine. Focused ultrasound that can open the blood brain barrier in targeted regions is also discussed (Bing et al., 2014) and would provide means to target hot spots and labyrinth paths selectively by local delivery of drugs. If the next generation of noninvasive devices due to model-based optimization of stimulations protocols has less adverse effects and becomes more efficient, patient groups with high frequency episodic migraine attacks and unsatisfactory treatment response will certainly be open to such a treatment.

The target structures that we suggest are like fingerprints, they are individual features of each migraine sufferer. The next step will be to provide individualized neural tissue simulations delivering the same output as clinical data. This can then serve as a test bed for exploring the use of personalized stereotactic neuromodulation.

DISCLOSURE/CONFLICT-OF-INTEREST STATEMENT

MAD has consulted for eNeura Inc in 2012.

ACKNOWLEDGMENTS

MAD kindly acknowledges helpful discussions with Paul van Valkenburgh, John Milton, and Claus Hilgetag.

Funding Bundesministerium für Bildung und Forschung (BMBF 01GQ1109).

REFERENCES

- Abramychiev, A. Y., Davydov, V., and Zykov, V. (1990). Drift of spiral waves on nonuniformly curved surfaces. *J. Exp. Theor. Phys.*, 70:666.
- Almeida, A. C. G., Texeira, H. Z., Duarte, M. A., and Infantesi, A. F. C. (2004). Modeling extracellular space electrodiffusion during Leao's spreading depression. *IEEE Trans Biomed Eng*, 51(3):450–458. Comparative Study.
- Amunts, K., Schleicher, A., Burgel, U., Mohlberg, H., Uylings, H. B., and Zilles, K. (1999). Broca's region revisited: cytoarchitecture and intersubject variability. *J Comp Neurol*, 412(2):319–341.
- Andrews, T. J., Halpern, S. D., and Purves, D. (1997). Correlated size variations in human visual cortex, lateral geniculate nucleus, and optic tract. *J Neurosci*, 17:2859–2868.
- Bangerth, W., Hartmann, R., and Kanschat, G. (2007). deal.II — a general purpose object oriented finite element library. *ACM Trans. Math. Softw.*, 33(4).
- Bing, C., Ladouceur-Wodzak, M., Wanner, C. R., Shelton, J. M., Richardson, J. A., and Chopra, R. (2014). Trans-cranial opening of the blood-brain barrier in targeted regions using a stereotaxic brain atlas and focused ultrasound energy. *Journal of Therapeutic Ultrasound*, 2(1):13.
- Blinder, P., Shih, A. Y., Rafie, C., and Kleinfeld, D. (2010). Topological basis for the robust distribution of blood to rodent neocortex. *Proceedings of the National Academy of Sciences*, 107(28):12670–12675.
- Bode, M. and Purwins, H. G. (1995). Pattern formation in reaction-diffusion systems-dissipative solitons in physical systems. *Physica D*, 86:53.
- Bojak, I., Oostendorp, T. F., Reid, A. T., and Kötter, R. (2010). Connecting mean field models of neural activity to EEG and fMRI data. *Brain Topogr*, 23(2):139–149.
- Bojak, I., Oostendorp, T. F., Reid, A. T., and Kötter, R. (2011). Towards a model-based integration of co-registered electroencephalography/functional magnetic resonance imaging data with realistic neural population meshes. *Philos Trans R Soc A*, 369(1952):3785–3801.
- Borsook, D., Aasted, C. M., Burstein, R., and Becerra, L. (2014). Migraine mistakes error awareness. *The Neuroscientist*, 20(3):291–304.
- Charles, A. C. and Baca, S. M. (2013). Cortical spreading depression and migraine. *Nat. Rev. Neurol.*
- Dahlem, M. A. (2013). Migraine generator network and spreading depression dynamics as neuromodulation targets in episodic migraine. *Chaos*, 23:046101.
- Dahlem, M. A. and Chronicle, E. P. (2004). A computational perspective on migraine aura. *Prog. Neurobiol.*, 74(6):351–361.
- Dahlem, M. A., Graf, R., Strong, A. J., Dreier, J. P., Dahlem, Y. A., Sieber, M., Hanke, W., Podoll, K., and Schöll, E. (2010). Two-dimensional wave patterns of spreading depolarization: retracting, re-entrant, and stationary waves. *Physica D*, 239:889–903.
- Dahlem, M. A. and Hadjikhani, N. (2009). Migraine aura: retracting particle-like waves in weakly susceptible cortex. *PLoS ONE*, 4:e5007.
- Dahlem, M. A. and Isele, T. M. (2013). Transient localized wave patterns and their application to migraine. *J. Math. Neurosci*, 3:7.

- Dahlem, M. A., Kurths, J., Ferrari, M. D., Aihara, K., Scheffer, M., and May, A. (2014). Understanding migraine using dynamical network biomarkers. *Cephalalgia*, online first.
- Dahlem, M. A. and Müller, S. C. (2003). Migraine aura dynamics after reverse retinotopic mapping of weak excitation waves in the primary visual cortex. *Biol. Cybern.*, 88:419–424.
- Dahlem, M. A. and Müller, S. C. (2004). Reaction–diffusion waves in neuronal tissue and the window of cortical excitability. *Ann. Phys.*, 13(7):442–449.
- Dahlem, M. A., Rode, S., May, A., Fujiwara, N., Hirata, Y., Aihara, K., and Kurths, J. (2013). Towards dynamical network biomarkers in neuromodulation of episodic migraine. *Transl. Neurosci.*, 4(3):282–294.
- Dahlem, M. A. and Tusch, J. (2012). Predicted selective increase of cortical magnification due to cortical folding. *J. Math. Neurosci.*, 2:14.
- Dale, A. M., Fischl, B., and Sereno, M. I. (1999). Cortical surface-based analysis. I. Segmentation and surface reconstruction. *NeuroImage*, 9(2):179–194.
- DaSilva, A. F., Granziera, C., Snyder, J., and Hadjikhani, N. (2007). Thickening in the somatosensory cortex of patients with migraine. *Neurology*, 69(21):1990–1995.
- Dasilva, A. F., Mendonca, M. E., Zaghi, S., Lopes, M., Dossantos, M. F., Spierings, E. L., Bajwa, Z., Datta, A., Bikson, M., and Fregni, F. (2012). tDCS-induced analgesia and electrical fields in pain-related neural networks in chronic migraine. *Headache*, 52(8):1283–1295.
- Davydov, V., Morozov, V., and Davydov, N. (2000a). Ring-shaped autowaves on curved surfaces. *Phys. Lett. A*, 267(5):326–330.
- Davydov, V. and Zykov, V. (1991). Kinematics of spiral waves on nonuniformly curved surfaces. *Physica D*, 49(1):71–74.
- Davydov, V. and Zykov, V. (1993). Spiral autowaves in a round excitable medium. *J. Exp. Theor. Phys.*, 76(3):414–419.
- Davydov, V. A., Manz, N., Steinbock, O., and Müller, S. C. (2002). Critical properties of excitation waves on curved surfaces: Curvature-dependent loss of excitability. *Europhys. Lett.*, 59:344–350.
- Davydov, V. A., Manz, N., Steinbock, O., Zykov, V. S., and Müller, S. C. (2000b). Excitation fronts on a periodically modulated curved surface. *Phys. Rev. Lett.*, 85:868–871.
- Davydov, V. A., Morozov, V. G., and Davydov, N. V. (2003). Critical properties of autowaves propagating on deformed cylindrical surfaces. *Physics Letters A*, 307:265–268.
- Diener, H.-C. (2013). *Novel Approaches in Migraine Treatment*. Future Medicine Ltd, London. doi:10.2217/9781780842349.
- Dreier, J. P. (2011). The role of spreading depression, spreading depolarization and spreading ischemia in neurological disease. *Nat. Med.*, 17:439–447.
- Famm, K., Litt, B., Tracey, K. J., Boyden, E. S., and Slaoui, M. (2013). Drug discovery: a jump-start for electroceuticals. *Nature*, 496(7444):159–161.
- Fischl, B., Sereno, M. I., and Dale, A. M. (1999). Cortical surface-based analysis. II. Inflation, flattening, and a surface-based coordinate system. *NeuroImage*, 9(2):195–207.
- Gao, Y., Green, S., and Drew, P. (2014). Cortical depth dependent hemodynamics to locomotion. *SfN abstract*.
- Gaschler-Markefski, B., Baumgart, F., Tempelmann, C., Schindler, F., Stiller, D., Heinze, H. J., and Scheich, H. (1997). Statistical methods in functional magnetic resonance imaging with respect to nonstationary time-series: auditory cortex activity. *Magn Reson Med*, 38(5):811–820.
- Gilissen, E. and Zilles, K. (1996). The calcarine sulcus as an estimate of the total volume of human striate cortex: a morphometric study of reliability and intersubject variability. *J Hirnforsch*, 37(1):57–66.
- Granziera, C., DaSilva, A. F., Snyder, J., Tuch, D. S., and Hadjikhani, N. (2006). Anatomical

- alterations of the visual motion processing network in migraine with and without aura. *PLoS medicine*, 3(10):e402.
- Grüsser, O.-J. (1995). Migraine phosphenes and the retino-cortical magnification factor. *Vision Res.*, 35(8):1125–1134.
- Hadjikhani, N. (2008). Relevance of cortical thickness in migraine sufferers.
- Hansen, J. M., Baca, S. M., VanValkenburgh, P., and Charles, A. (2013). Distinctive anatomical and physiological features of migraine aura revealed by 18 years of recording. *Brain*, 136(12):3589–3595.
- Hilgetag, C. C. and Barbas, H. (2005). Developmental mechanics of the primate cerebral cortex. *Anatomy and embryology*, 210(5-6):411–417.
- Hübel, N. and Dahlem, M. A. (2014). Dynamics from seconds to hours in Hodgkin–Huxley model with time–dependent ion concentrations and buffer reservoirs. *accepted for PLoS Comp. Biol.*
- Hübel, N., Schöll, E., and Dahlem, M. A. (2014). Bistable dynamics underlying excitability of ion homeostasis in neuron models. *PLoS Comp. Biol.*, 10:e1003551.
- Karatas, H., Erdener, S. E., Gursoy-Ozdemir, Y., Lule, S., Eren-Kocak, E., Sen, Z. D., and Dalkara, T. (2013). Spreading depression triggers headache by activating neuronal Panx1 channels. *Science*, 339(6123):1092–1095.
- Kim, J. S., Singh, V., Lee, J. K., Lerch, J., Ad-Dab’bagh, Y., MacDonald, D., Lee, J. M., Kim, S. I., and Evans, A. C. (2005). Automated 3-D extraction and evaluation of the inner and outer cortical surfaces using a Laplacian map and partial volume effect classification. *NeuroImage*, 27(1):210–221.
- Kneer, F., Schöll, E., and Dahlem, M. A. (2014). Nucleation of reaction-diffusion waves on curved surfaces. *New J. Phys.*, 16:053010.
- Kozloski, J. and Wagner, J. (2011). An ultrascale solution to large-scale neural tissue simulation. *Frontiers in neuroinformatics*, 5.
- Krieg, T. D., Salinas, F. S., Narayana, S., Fox, P. T., and Mogul, D. J. (2013). Pet-based confirmation of orientation sensitivity of tms-induced cortical activation in humans. *Brain stimulation*, 6(6):898–904.
- Krischer, K. and Mikhailov, A. S. (1994). Bifurcation to traveling spots in reaction-diffusion systems. *Phys. Rev. Lett.*, 73(23):3165–3168.
- Lipton, R. B., Dodick, D. W., Silberstein, S. D., Saper, J. R., Aurora, S. K., Pearlman, S. H., Fischell, R. E., Ruppel, P. L., and Goadsby, P. J. (2010). Single-pulse transcranial magnetic stimulation for acute treatment of migraine with aura: a randomised, double-blind, parallel-group, sham-controlled trial. *Lancet Neurol.*, 9:373–380.
- Lotze, M., Erb, M., Flor, H., Huelsmann, E., Godde, B., and Grodd, W. (2000). fMRI evaluation of somatotopic representation in human primary motor cortex. *Neuroimage*, 11(5 Pt 1):473–481.
- Maekawa, T. (1996). Computation of shortest paths on free-form parametric surfaces. *Journal of mechanical design*, 118(4):499–508.
- Magid, E., Soldea, O., and Rivlin, E. (2007). A comparison of gaussian and mean curvature estimation methods on triangular meshes of range image data. *Comput Vis Image Underst.*, 107:139–159.
- Magis, D., Gérard, P., and Schoenen, J. (2013). Transcutaneous vagus nerve stimulation (tvns) for headache prophylaxis: initial experience. *J Headache Pain*, 1(Suppl 1):P198.
- Manz, N., Davydov, V., Müller, S. C., and Bär, M. (2003). Dependence of the spiral rotation frequency on the surface curvature of reaction–diffusion systems. *Phys. Lett. A*, 316(5):311–316.
- Manz, N. and Müller, S. (2003). Fabrication of quasi-two-dimensional, heterogeneously curved

- belousov–zhabotinsky systems. *Review of scientific instruments*, 74(12):5161–5166.
- Maselko, J. and Showalter, K. (1989). Chemical waves on spherical surfaces. *Nature*, 339(6226):609–611. 10.1038/339609a0.
- Mikhailov, A. S., Davydov, V. A., and Zykov, V. S. (1994). Complex dynamics of spiral waves and motion of curves. *Phys. D*, 70(1-2):1–39.
- Miura, R. M., Huang, H., and Wylie, J. J. (2007). Cortical spreading depression: An enigma. *Eur. Phys. J. Spec. Top.*, 147(1):287–302.
- OpenCFD Ltd (ESI Group) (2014). OpenFOAM.
- Pöppel, E. (1973). Fortification illusion during an attack of ophthalmic migraine. Implications for the human visual cortex. *Naturwissenschaften*, 60:554–555.
- Postnov, D. E., Muller, F., Schuppner, R. B., and Schimansky-Geier, L. (2009). Dynamical structures in binary media of potassium-driven neurons. *Phys Rev E Stat Nonlin Soft Matter Phys*, 80(3 Pt 1):031921.
- Postnov, D. E., Postnov, D. D., and Schimansky-Geier, L. (2012). Self-terminating wave patterns and self-organized pacemakers in a phenomenological model of spreading depression. *Brain Res.*, 1434:200–211.
- Rademacher, J., Morosan, P., Schormann, T., Schleicher, A., Werner, C., Freund, H. J., and Zilles, K. (2001). Probabilistic mapping and volume measurement of human primary auditory cortex. *Neuroimage*, 13(4):669–683.
- Rajkowska, G. and Goldman-Rakic, P. S. (1995). Cytoarchitectonic definition of prefrontal areas in the normal human cortex: II. Variability in locations of areas 9 and 46 and relationship to the Talairach Coordinate System. *Cereb Cortex*, 5(4):323–337.
- Richter, F. and Lehmenkühler, A. (1993). Spreading depression can be restricted to distinct depths of the rat cerebral cortex. *Neuroscience letters*, 152(1):65–68.
- Roland, P. and Zilles, K. (1998). Structural divisions and functional fields in the human cerebral cortex. *Brain Res Brain Res Rev.*, 26:87–105.
- Santos, E., Schöll, M., Sánchez-Porrás, R., Dahlem, M. A., Silos, H., Unterberg, A., Dickhaus, H., and Sakowitz, O. W. (2014). Radial, spiral and reverberating waves of spreading depolarization occur in the gyrencephalic brain. *NeuroImage*.
- Schenk, C. P., Or-Guil, M., Bode, M., and Purwins, H. G. (1997). Interacting pulses in three-component reaction-diffusion systems on two-dimensional domains. *Phys. Rev. Lett.*, 78:3781.
- Schipper, S., Riederer, F., Sándor, P. S., and Gantenbein, A. R. (2012). Acute confusional migraine: our knowledge to date.
- Smith, S. M., Jenkinson, M., Woolrich, M. W., Beckmann, C. F., Behrens, T. E., Johansen-Berg, H., Bannister, P. R., De Luca, M., Drobnjak, I., Flitney, D. E., Niazy, R. K., Saunders, J., Vickers, J., Zhang, Y., De Stefano, N., Brady, J. M., and Matthews, P. M. (2004). Advances in functional and structural MR image analysis and implementation as FSL. *NeuroImage*, 23 Suppl 1:S208–219.
- Stensaas, S. S., Eddington, D. K., and Dobelle, W. H. (1974). The topography and variability of the primary visual cortex in man. *J Neurosurg*, 40(6):747–755.
- Stovner, L., Hagen, K., Jensen, R., Katsarava, Z., Lipton, R., Scher, A., Steiner, T., and Zwart, J. A. (2007). The global burden of headache: a documentation of headache prevalence and disability worldwide. *Cephalalgia*, 27(3):193–210.
- Strogatz, S. H. (1994). *Nonlinear Dynamics and Chaos*. Westview Press, Cambridge, MA.
- Thompson, P. M., Schwartz, C., Lin, R. T., Khan, A. A., and Toga, A. W. (1996). Three-dimensional statistical analysis of sulcal variability in the human brain. *J. Neurosci.*, 16(13):4261–4274.
- Tuckwell, H. C. (1981). Simplified reaction-diffusion equations for potassium and calcium ion concentrations during spreading cortical depression. *Int. J. Neurosci.*, 12:95–107.

- Tuckwell, H. C. and Miura, R. M. (1978). A mathematical model for spreading cortical depression. *Biophys. J.*, 23:257–276.
- Versteeg, H. and Malalasekera, W. (1995). An Introduction to CFD. The Finite Volume Method.
- Vincent, M. and Hadjikhani, N. (2007). Migraine aura and related phenomena: beyond scotomata and scintillations. *Cephalalgia*, 27:1368–1377.
- Walters, N. B., Egan, G. F., Kril, J. J., Kean, M., Waley, P., Jenkinson, M., and Watson, J. D. G. (2003). In vivo identification of human cortical areas using high-resolution MRI: an approach to cerebral structure-function correlation. *Proc Natl Acad Sci U S A*, 100(5):2981–2986.
- Watson, J. D., Myers, R., Frackowiak, R. S., Hajnal, J. V., Woods, R. P., Mazziotta, J. C., Shipp, S., and Zeki, S. (1993). Area V5 of the human brain: evidence from a combined study using positron emission tomography and magnetic resonance imaging. *Cereb Cortex*, 3(2):79–94.
- Wilkinson, F. (2004). Auras and other hallucinations: windows on the visual brain. *Prog. Brain Res.*, 144:305–320.
- Woitzik, J., Hecht, N., Pinczolits, A., Sandow, N., Major, S., Winkler, M. K., Weber-Carstens, S., Dohmen, C., Graf, R., Strong, A. J., et al. (2013). Propagation of cortical spreading depolarization in the human cortex after malignant stroke. *Neurology*, 80(12):1095–1102.
- Zandt, B.-J., ten Haken, B., van Putten, M. J., and Dahlem, M. A. (2015). How does Spreading Depression Spread? - Physiology and Modeling. *in preparation*.